Computers in Biology and Medicine 40 (2010) 456–463

Contents lists available at ScienceDirect

Computers in Biology and Medicine

journal homepage: www.elsevier.com/locate/cbm

Implementation of a novel interpolating method to epicardial potential mapping for atrial fibrillation study

Weijia Lu [a], Cuiwei Yang [b], Zuxiang Fang [b], Xingpeng Liu [c], Xin Zhu [a], Daming Wei [a,*]

[a] Department of Information Systems, Aizu University, Aizu-Wakamatsu, Fukushima-ken 965-8580, Japan
[b] Department of E.E, Fudan University, Shanghai 200-433, PR China
[c] Department of Cardiology Center for Atrial Fibrillation, Beijing Anzhen Hospital, Capital Medical University, Beijing 100-029, PR China

ARTICLE INFO

Article history:
Received 5 September 2009
Accepted 25 February 2010

Keywords:
Atrial fibrillation
Epicardial mapping
3D interpolation
Local excitation time

ABSTRACT

Epicardial potential mapping is an efficient way to visualize the potential distribution on the epicardial surface. We found in our previous study, that the traditional linear interpolation used for the epicardial mapping may cause errors and distortions in reconstruction of the electric activities on the epicardial surface especially during the atrial fibrillation. In this study, we devoted on the implementation of a 3D interpolating method, and verified it in comparison with another interpolating method as well as studying of the mechanism of vagal atrial fibrillation (AF). In case studying, we analyzed the epicardial data from seven canine cardiac models using this method and found the macro-re-entry during the sustainable AF is more likely due to the dispersion of refractoriness in the myocardium and does not demonstrated the focal patterns at the beginning of AF. This indicated that the electrophysiological characteristics of myocardium might have been changed during the paroxysmal atrial fibrillation (PAF).

1. Introduction

The epicardial potential mapping is widely used in the electrophysiological study to analyze the cardiac electrical activities through visualizing the ECG potential distribution on the epicardium. Due to the sparsity of electrodes on the epicardial surface, the epicardial potential mapping is usually conducted using a linear interpolating method with a light computation complexity [1]. In our previous research, we developed a novel epicardial mapping system which can visualize the isopotential maps offline [2–4]. In that system, we used a linear interpolating method based on the Euler distance and the included angles [5]. We tested the whole system in several animal experiments and found the isopotential map working satisfactorily during the sinus (SN) rhythm but poorly during the AF. In AF rhythm, the activation propagation was not as obvious as it in sinus rhythm on the 3D geometric model [5]. We have confirmed that this problem is caused by the estimation error of the linear interpolation as explained by Ni et al. [6]. In this paper, we proposed a 3D interpolating method composed of the muscle noise removing, the interpolation-base triangle forming, the local activation time extracting, the local waveform shifting and alignment proposed in the Ni et al.'s study [6] and the waveform estimating on the whole geometric model. In the later part of this study, we evaluated it in a case study and tried to reveal the mechanism of vagal atrial fibrillation.

2. Methods

2.1. Problem's survey and theory's revisiting

In our epicardial mapping system, a 3D geometric model of atrium composed of 3136 vertexes and 6234 faces is created by 3DS MAX and stored in the ASE file [5]. The electrodes are sparsely distributed on these faces, the coordinates of which are stored in the POLE file [5]. The interpolation problem is to estimate the potential on each vertex of the geometric model from the potential on the electrode.

Ni et al.'s study gives a profound discussion about the abrupt change in potential in the vicinity of the activation wave front, and brings forward a local activation time alignment methods to improve the interpolation result over standard linear techniques [6]. This method is based on two notions: (1) the propagation speed in normal tissue with electrode spacing ranging from 1.5 to 7.5 mm (the space in our system is from 1.5 to 5 mm), is locally constant and thus activation time varies linearly in space; (2) the wave form morphology is relatively similar in the region between sampling electrodes [6]. In this paper, we adopted local activation time alignment into our interpolating method (Section 2.6), which contains else previous steps, i.e. the muscle noise removing

* Corresponding author.
E-mail addresses: AlfredWJLu@gmail.com (W. Lu), dm-wei@u-aizu.ac.jp (D. Wei).

0010-4825/$ - see front matter © 2010 Elsevier Ltd. All rights reserved.
doi:10.1016/j.compbiomed.2010.02.010

(Section 2.2), the interpolation based triangle retrieving (Section 2.3) and the estimating of the activation time of myocardium at each electrode (Section 2.4).

2.2. Removing the muscle noise

The retrieved epicardial ECGs by our mapping system are free of the baseline drifting as well as the power noise [3], but full of the muscle noise. Because its spectral depends on the muscle tremor and the electrode–muscle connection, which both increase the difficulty of modelling the noise's characteristics and designing a statistical filter to remove it. In our implementation, simple wavelet shrinkage methods is applied to the noisy data [7]. The noise signal is transformed into the wavelet domain using a trous wavelet transform based on a biorthogonal wavelet with two vanishing moments (bior2.6). A trous wavelet transform is a kind of time-shift-invariant wavelet representation and is massively used in the noise suppression [8] comparing with the pyramid decomposition method [9]. The latter one is acknowledged as a none time-shift-invariant one. The wavelet coefficients on six scales are subjected to soft minmax thresholding, with the threshold $Th=\sigma(0.3936+0.1829\log_2(n))u(n-32)$, where the $u(n)$ is the step function. And the result is then inverse-transformed, and restored as the input of the interpolating method. In order to determine the threshold, an estimation of the noise's variance is necessary, which can be expressed as $\hat{\sigma}=median(|d|)/0.6745$, where the $median(\cdot)$ operator is to retrieve the median of a finite list of numbers, and d is the detail coefficients on all scales.

Fig. 1 demonstrates the denoising results on in vivo animal experiments, while the Figs. 2a–d compares the denoising effects in different wavelet and threshold. It is obvious that the minmax threshold combined with the bior2.6 wavelet is the appropriate choice on different SNR condition.

2.3. Forming the interpolation-base triangle for each geometric vertex

The same method detail described in our previous studies is used in forming the interpolation-base triangle [4]. At first, the three vertexes of the triangle, which are the central points of three electrodes, are determined for each vertex. The vertex of the interpolation-based triangle is called the electrode vertex in this study to distinguish from the vertex of geometric models. The first electrode vertex of the interpolation-base triangle is the center of the electrode, which has the smallest Euler distance to the specified vertex (e.g. the 0th electrode vertex in Fig. 3). And the other two electrode vertexes of the interpolation-base triangle have the smallest included angle with the special vertex and the first electrode vertex (e.g. the 1st and the 2nd electrode vertex in Fig. 3) [4,5].

2.4. Estimating the activation time of myocardium at three electrodes in a so-called interpolation-base triangle

Based on Ni's theory, we should estimate the activation time of the myocardium at the three electrodes in the interpolation-based triangle [6]. The parsing of the excitation time has been discussed in a lot of studies [11–13], in which the points with the minimum first derivative in the extracellular unipolar electrogram are usually recommended as the characteristic points to determine the activation time. Unfortunately, to precisely locate them is proved to be difficult when some fractional artifacts exists on the baseline, see Figs. 1 and 4c. To decrease or even eliminate the influence from these fractional artifacts, we add an extra preprocessing step to extract the up-down envelopes of the epicardial ECG signals after removing the muscle noise. In our study, a unique point with a minimum first derivative is determined between each positive extreme in the up envelope and the corresponding negative counterpart in the down envelope. This procedure is employed due to the fact that the positive extremes on fractional artifacts are usually smaller than the preceding activation waveforms, which contains the minimum first derivative corresponding to the local excitation times. Fig. 4 demonstrate the locating procedure.

Till this step, we have (a) the interpolation-base triangle for each vertex of the geometric model, (b) the local excitation time sequence at each electrode vertex of the interpolation-base triangle.

2.5. Estimating the activation time of myocardium at a geometric mode's vertex and forming the alignment windows for each electrode vertexes

As it is supposed that the propagation velocity is uniform within the interpolation-base triangle [6], the excitation time of myocardium at a geometric model's vertex could to be precisely determined by using the linear interpolating method in Eq. (1),

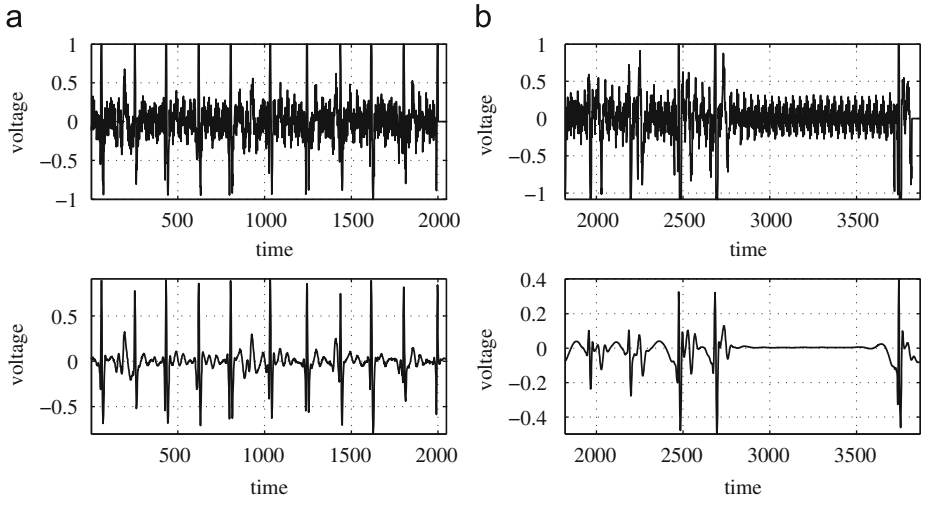

Fig. 1. Demonstration of muscle noise removing on in vivo animal experiment records: (a) Canine's heart is in the normal SN rhythm and (b) Canine's heart is suffering onset of atrium tachyarrhythmia.

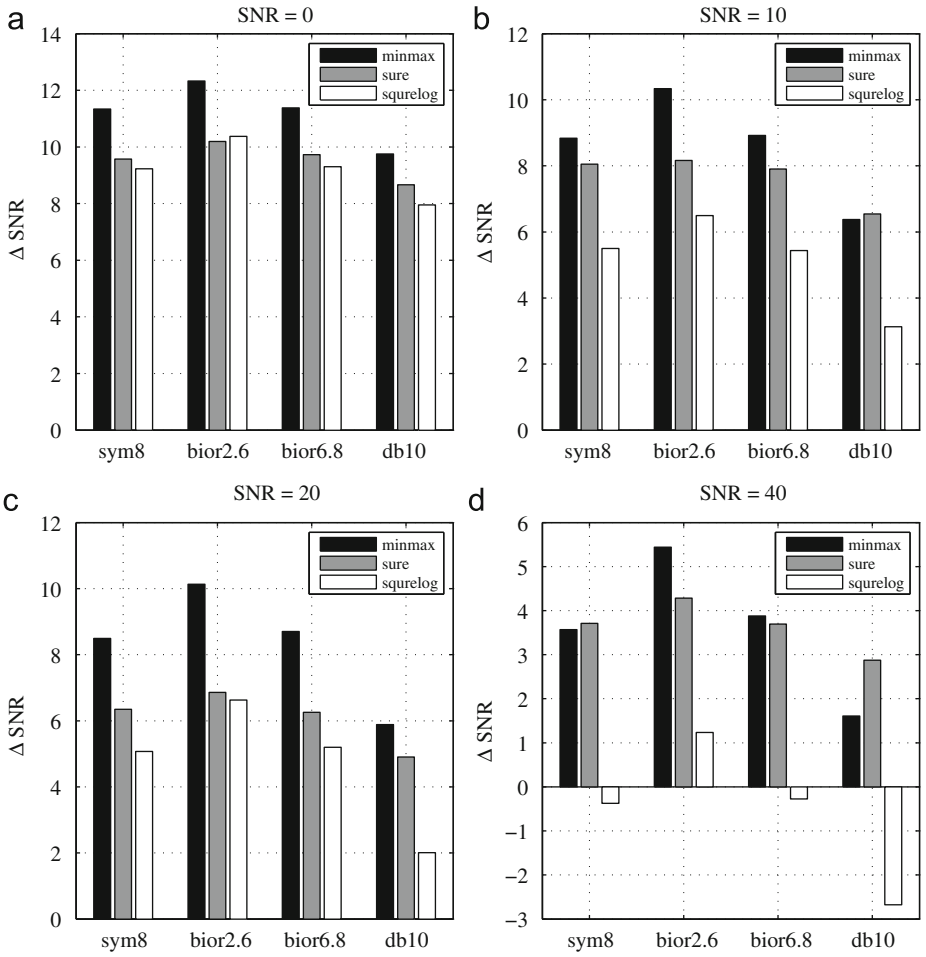

Fig. 2. Comparing the denoising effect in different wavelet and threshold ($p < 0.01$). The uncontaminated signal is epicardial signal produced by CardiacMaster [10], the AWGN's variance can be calculated corresponding to the given SNR, and the $SNR = 20\log(P_{signal}/P_{noise})$. In the denoising processing, the noise's variance is estimated through the detail coefficients.

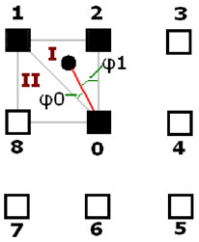

Fig. 3. Determining the interpolation-based triangle for a specified vertex. The little dot is the vertex of the geometric models. The 0th electrode vertex is the one which has the smallest Euler distance to the specified vertex. $\varphi 0$ and $\varphi 1$ are two included angles. And the first and the second electrode vertex are another two to form a unique interpolation-based triangle.

where n is the index of vertex, N is the number of electrode vertex forming the triangle ($N=2$ if there are not enough electrode vertex to form an interpolation-base triangle, else $N=3$, refer to the description in [5]), S_i^e is the Euler distance between the vertex and i th electrode's central point, T^e is the activation time of myocardium at the electrode while the T^v is that at the vertex.

$$T_n^v = \sum_{i=1}^{N} \frac{T_i^e}{S_i^e} \Big/ \sum_{i=1}^{N} \frac{1}{S_i^e} \tag{1}$$

In each iteration of interpolation, the interpolation-base triangle is defined to be newly activated as the myocardium at any electrode vertex forming this triangle is excited. When all electrode vertexes forming this triangle return to the resting status, an activation period can be constructed as well as the alignment windows on these electrode vertexes. Before the all electrode vertexes returning to the resting status, the triangle is called already activated.

An electrode, where the myocardium is activated earlier than or simultaneously with that at the vertex, is named the pre-activated electrode, and the post-activated electrode *vice verse*. The alignment window's lengths on these two kinds of electrode vertexes are defined differently. The length of the former is in Eq. (2), the latter in Eq. (3), where L_j is the length of alignment window on j th electrode vertex, L_{ap} is the length of activation period on this triangle, L_j^b is the addition for alignment on the post-activated electrode.

$$L_j = L_{ap} = \max(T^e_{i=1\ldots N}) - \min(T^e_{i=1\ldots N}) + 1 \tag{2}$$

$$L_j = L_{ap} + L_j^b = \max(T^e_{i=1\ldots N}) - \min(T^e_{i=1\ldots N}) + 1 + (T_j^e - T_n^v) \tag{3}$$

2.6. Estimating the potential at the vertex of geometric model after shifting the waveforms in alignment windows

After the alignment windows have been calculated, the waveform measured at each electrode forming the triangle is shifted in such a way that its activation time will finally align to the estimated activation time at the vertex [6]. This process is based on the hypothesis that the electrogram morphology varies

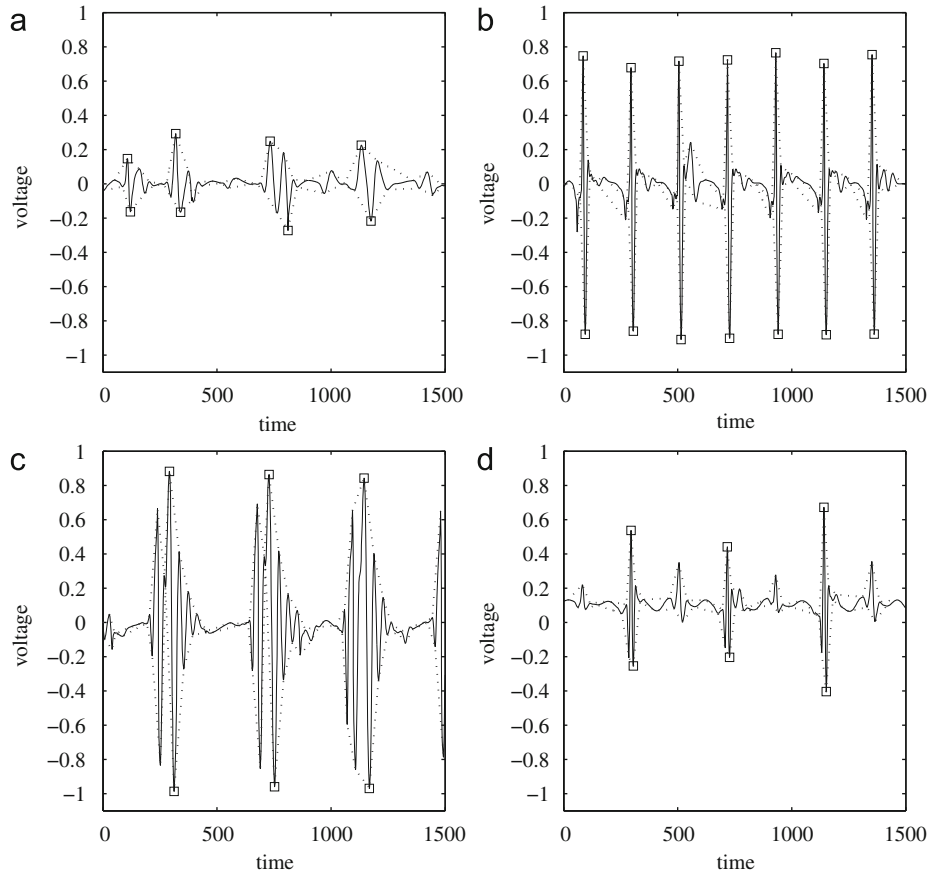

Fig. 4. Demonstration of marking the positive and negative extremes on in vivo animal experiment records. The signals fed into this procedure are free of muscle noise. The dotted lines indicate the up-down envelopes and the square marks indicate the positive-negative extremes, the minimum first derivative between each pair is the location of local activation time of myocardium: (a) extracted from left atrium appendage, (b) extracted from right atrial posterior region, (c) extracted from the right atrium appendage, this record is full of fractional artifacts and (d) extracted from the right pulmonary vein, discernable ventricular remote complex interlaced with atrial deflection.

relatively modestly in the neighbourhood of local region except for a time shift in the potential waveforms [6]. After alignment, an interpolation is performed on each set of meta data on the alignment window as we did in former studies [4,5]: the potential at a geometric model's vertex is calculated from the weighted sum of the aligned measured potential at the three electrode vertexes of its interpolation-base triangle.

3. Program schematic

Fig. 5 demonstrates the dynamic model of the interpolating method described above. The raw signals in an epicardial record are discretized as samples, and each sample contains 128 meta values (short integer), one for each channel. After the whole record (or may be a segment of it) is stored in memory, a transposing of meta values is performed at the beginning of pre-interpolation, so that they will be sequenced along channels. After pre-interpolation, an interpolation thread is created and fed by 128 meta values, i.e., a single sample, in each interpolating iteration, until a terminating signal is received to indicate the end of record or an unexpected stopping request (usually generated by the GUI event initiated by user). When the terminating signal arrives, the process collects the ECG signal sequences on the vertexes of all interpolation-base triangles for the rendering of the 3D model (Fig. 5c).

In this research, we employed the differential method to localize the local extreme in the ECG signals, and we named this procedure as "find the extreme" (Fig. 5b). In the preprocessing, to suppress the fractional artifacts as many as possible, we repeatedly extract envelopes for $T_{\_recurvate}$ times. Furthermore, the repository period has an explicit electrophysiological meaning and is used as a threshold in the time domain (*Rep* in Fig. 5a). Hence, the repository period's value should be updated at the beginning of each iteration as well as the mean altitude of the selected extremes (V th in Fig. 5a) and the mean altitude of all candidates ($V_{\_avg}$ in Fig. 5a).

If the interpolation-base triangle of a vertex is neither the newly activated nor the already activated, the interpolation described in previous research [4,5] is performed immediately (Fig. 5c). If the three electrodes, whose central locations are the three vertexes of the interpolation-base triangle, are activated at the same time, the alignment windows of these electrodes are set as full right after the procedure: set alignment window for this triangle and align pre-activated electrodes. In such a condition, the interpolation is performed immediately on these alignment windows in the current iteration.

4. Computation complexity

As the interpolating algorithm is used in a realtime epicardial mapping system [4]. The computation complexity of it should be

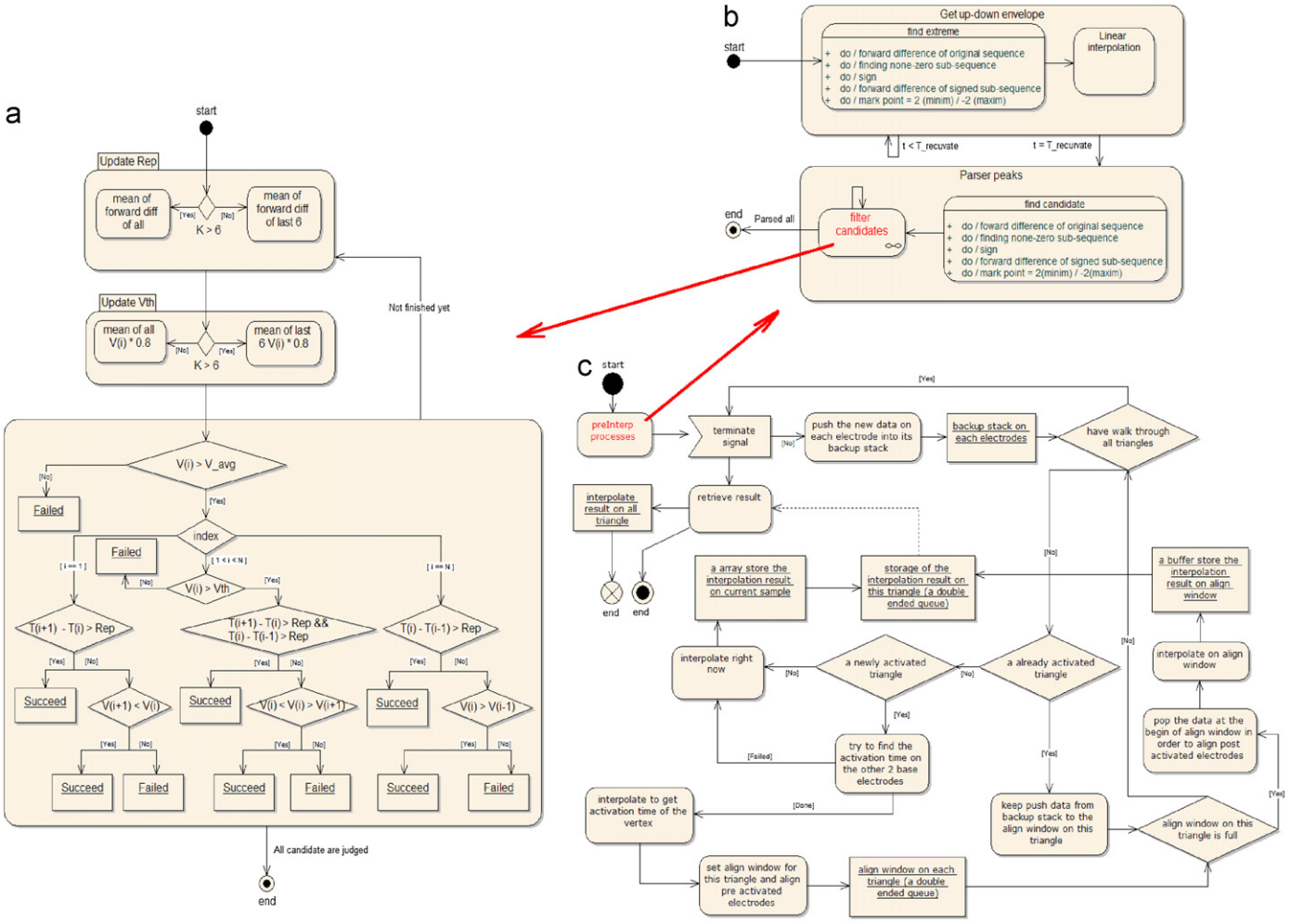

Fig. 5. The dynamic model describing the algorithm used in this study: (a) filtering the positive extremes belonging to the characteristic waveforms from all the up envelope, (b) retrieving the local positive–negative extremes' pairs of the characteristic waveforms to locate the excitation times on all electrodes and (c) interpolating the distribution of potential on the epicardial surface.

discussed comparing with the linear one proposed in our previous research [4,5]. The additional cost of the new method mainly exists in the steps of the localization of the local activation times and the alignment of the waveforms on electrodes.

If the length of meta data on each channel in an epicardial record is n, the $T\_recurvate$ for recurrently extracting envelopes is c, and we linearly interpolate on the local extremes with the interlacing distance of k_i ($\sum k_i = n$), the computation complexity of the activity named "Get up-down envelope" is

$$C(n) = T1 + T2 \times 2 + (T1 + T2) \times (c-1) = \Theta(n) + \Theta(n) \times 2 + \Theta(n) \times (c-1) = \Theta(n) \quad (4)$$

where $T1$ is the cost on finding extremes and $T2$ the cost on the linear interpolation of up or down extremes. As the number of retrieved candidates in activity named "Parser peaks" is always smaller than n, the computation complexity of this activity is

$$C(n) = (T1 + T2) \times 2 = \Theta(n) + O(n) = \Theta(n) \quad (5)$$

where $T1$ is the cost on finding candidates and $T2$ is the cost on filtering candidates. The computation complexity on locating the minimum derivative points between each local positive-negative extremes' pair on up-down envelopes is (if the sum of them is l, and the distance between two successive pairs is n_k)

$$C(n) = \sum_{k=1}^{l} \Theta(n_k) = O(n) \left(\text{because } \sum_{k=1}^{l} n_k < n \right) \quad (6)$$

Considering Eqs. (4), (5) and (6), the additional cost in preprocessing for localization of the local activation times is $128 \times \Theta(n) = \Theta(n)$.

In the alignment of the waveforms measured on electrodes in each iteration of interpolation, the computation complexity for two special activities' sequences are required. One is to search a newly activated triangle and includes the activities named "try to find the activation time on the other 2 base electrodes", "interpolate to get activation time of the vertex", and "set alignment window for this triangle and align pre-activated electrodes", respectively. If the length of the local excitation time sequence on the electrode is $m (m < n)$ and the binary tree is used in the 1st activity, the searching time on this sequence could be $O(\log(m))$. Then, the computation complexity in the 3rd activity is determined by the span between the activation time on the pre-activated electrode and the activation time on the vertex. This span follows the uniform distribution $U(0,n)$. Accordingly, the mean cost in the alignment for a pre-activated

electrode can be $\Theta(n/2)$. Therefore, in this sequence, for all the M interpolation-base triangles, the additional cost is (N is as usual the sum of electrodes forming the triangle, n is the length of record, N' is the sum of pre-activated electrodes, usually $N' < N$)

$$C(n) = M \times \left(\sum_{k=1}^{N} O(\log(m_k)) + \Theta(1) + \sum_{k=1}^{N'} \Theta(n/2) \right) < 2MO(\log(n)) + 2MO(n/2) = MO(n) \quad (7)$$

The other sequence is related to the fullness of all alignment windows on the interpolation-base triangle. This path consists of two activities, named "pop the data at the begin of alignment window in order to align post-activated electrodes" and "interpolate on alignment window". The computation complexity on this path can be easily proved to be

$$C(n) = M \times (\Theta(n/2) + \Theta(n/2)) = M\Theta(n) \quad (8)$$

Considering Eqs. (7) and (8), the additional cost in each iteration should be no more than $M\Theta(n)$.

5. Evaluation the interpolation performance

5.1. Comparing the results using interpolating methods with and without the alignment

Fig. 6a illustrates the epicardial ECG waveforms measured from the three electrodes, whose central points are the electrode vertexes of a interpolation-based triangle. Fig. 6b shows the interpolating result at the observation vertex using the methods with (aligned) and without (unaligned) the local action time alignment. It is apparent that the waveform estimated from the interpolating method without the action time alignment contains unacceptable distortion (the first cycle) and errors (the third cycle), marked in red. Therefore, our interpolating method introduced in this study is more feasible for the estimation of epicardial potential distribution compared with the one we used in previous study [4,5].

5.2. Comparing our interpolating method with B-spline interpolating

Eight different records are random selected as test set from 47 epicardial ECGs in AF condition and 30 epicardial ECGs in SN. Two electrodes acting as the fake geometric vertexes are selected from the electrode patches, which are sutured on the two flat topography on atrium surface (left atrium appendage and right atrium appendage). The adjacency relationship among the fake geometric vertex and their nearby ones are modified to simulate the topology in Fig. 3. The estimated epicardial ECG on the fake geometric vertex is denoted as V^e, while the real measured one is V^m. We use two indicators *RE* and *RMSE* defined as following to measure the error of estimation [6]:

$$RE = \sqrt{\frac{\sum_{i=1}^{N}(V_i^e - V_i^m)^2}{\sum_{i=1}^{N}(V_i^m)^2}} \quad (9)$$

$$RMSE = \sqrt{\frac{\sum_{i=1}^{N}(V_i^e - V_i^m)^2}{N}} \quad (10)$$

where N is the total samples in a set records, in the experiment, it is 20000. Comparing our interpolating method with the B-spline interpolating [14], we have Table 1.

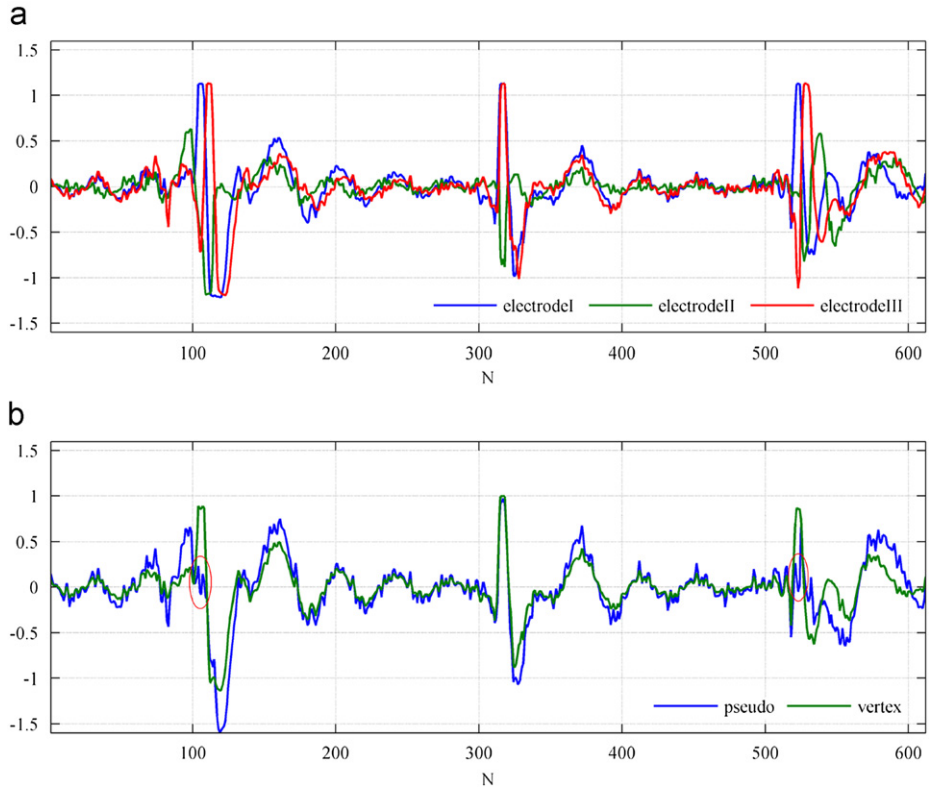

Fig. 6. The comparison the interpolation results using the methods with and without the local action time alignment: (a) the epicardial ECG waveforms measured at three electrode vertexes and (b) the "unaligned" waveform is the direct weighted sum of the epicardial ECG at the three electrode vertexes, as we did in [4,5], and the "aligned" waveform is the interpolating results estimated with the alignment procedure. The unit in the x axis is sample (1/2000 Hz = 0.5 ms) and all the ECG waveforms are scaled for demonstrations.

Table 1
Comparing our method with B-spline.

Record	$\Delta RE(\%)$[a]	$\Delta RMSE(\%)$[b]
Fake vertex (=26) at right atrium appendage		
1	9.9078	3.2047
2	9.0357	3.1506
3	8.2381	2.6584
4	3.9773	2.2996
5	5.2881	4.4587
6	8.8250	10.2545
7	2.8059	3.5784
8	4.5868	5.6895
Fake vertex (=53) at left atrium appendage		
1	9.3883	6.9653
2	9.3673	6.4796
3	5.4860	5.3964
4	1.8460	2.9034
5	3.2015	4.6764
6	8.8153	5.8994
7	2.0154	3.8456
8	3.3654	5.0467

[a] $\Delta RE = (RE_{Bspline} - RE_{ours})/RE_{Bspline}$.
[b] $\Delta RMSE = (RMSE_{Bspline} - RMSE_{ours})/RMSE_{Bspline}$.

6. A case study for analyzing vagal AF

We employed this interpolating method to reconstruct the 3D epicardial potential maps to study the mechanism of the vagal AF. Chen reviewed the clinical literature dealing with the relationship between the autonomic nervous system and AF [15]. Lombardi have proved that one-third of paroxysmal atrial fibrillation (PAF) is predominated by the vagal activation [16]. The vagal ganglia mainly distributes in three anatomical positions: the SVC-Ao fat pad, the RPV fat pad, and the IVC-LA fat pad [17]. We use the same methodology reported in Scherlag's study [18]: to stimulate the PRV fat pad which locates between the vena cava and the right superior pulmonary vein. Stimulation on it will shorten effective refractory period (ERP) [17] and therefore eases the induction of PAF.

In this study, we used seven canine cardiac models to analyze the mechanism of vagal AF. The average body weight of these mongrel dogs is 15–25 kg. Before the experiment, these dogs were anesthetized by intravenous injection with pentobarbital sodium, and their hearts were exposed by median sternotomy incising. During the experiment, we use signal APDs to induce AF (10 V, 20 Hz, duration square wave pulses 0.2 ms). The epicardial signals were simultaneously recorded at both sides of the atrium appendage, i.e. left atrium appendage (ALA) and right atrium appendage (ARA), at both sides of the atrial posterior region, i.e. the left and right atrial posterior region (PLA and PRA) as well as the surfaces of four pulmonary veins (PVs), i.e. the superior of left pulmonary vein (LSPV), the inferior of left pulmonary vein (LIPV), the superior of right pulmonary vein (RSPV), and the inferior of right pulmonary vein (RIPV). The specifications of the inter-electrode space are as follows: ALA and ARA 5×5 (mm), PLA and PRA 4×4 (mm), surrounding PV 1.5×3.5 (mm). The diameter of each electrode is 1.2 mm, and the height is 0.16 mm(+0.10/−0.03 mm). These electrodes on 3–4 soft patches were sutured onto the atrium surface before the whole mapping system worked. The detected epicardial potential signals of 128 channels were transmitted to PC and displayed on the screen [4]. The sample frequency of each channel is 2 kHz and the throughput rate of sample data acquisition system is 400 kHz for 12 bits, i.e. the average data transmission speed is about 3 Mbps. Before being transmitted to PC, the raw epicardial potential signals have been pre-filtered and band trapped, thus the frequency spectrum of the preprocessed signals extends from 40 to 600 Hz except 50 Hz, which is removed using a power-frequency notch filter. The local activation times of the myocardium at each channel in the epicardial records are parsed, meta data on these channels are interpolated, and the interpolated results are rendered on a 3D geometric model by using *OpenGL*® [4].

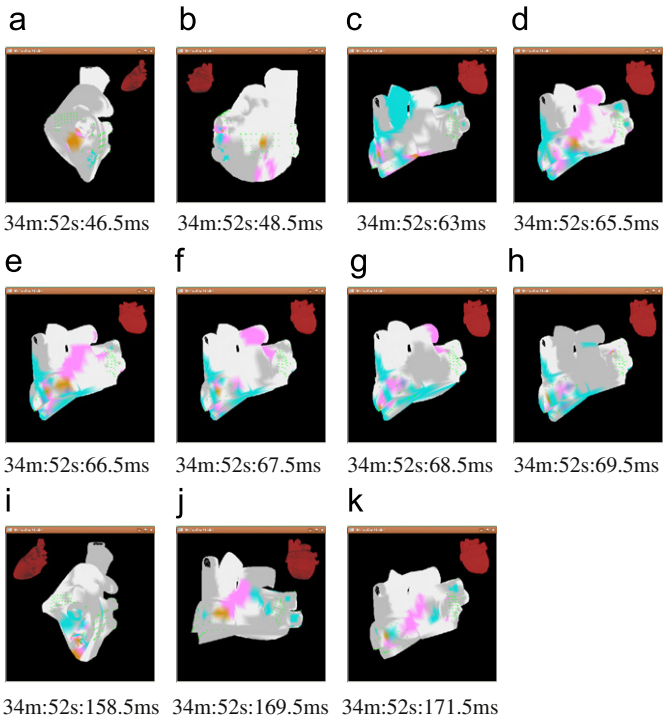

Fig. 7. Potential distribution at the beginning of PAF induced by vagal simulation. Yellow region indicates the location of the activation wave front: (a) 34 min:52 s:46.5 ms, (b) 34 min:52 s:48.5 ms, (c) 34 min:52 s:63 ms, (d) 34 min:52 s:65.5 ms, (e) 34 min:52 s:66.5 ms, (f) 34 min:52 s:67.5 ms, (g) 34 min:52 s:68.5 ms, (h) 34 min:52 s:69.5 ms, (i) 34 min:52 s:158.5 ms, (j) 34 min:52 s:169.5 ms and (k) 34 min:52 s:171.5 ms. (For interpretation of the references to colour in this figure legend, the reader is referred to the web version of this article.)

In one canine cardiac model, we detected a PAF lasting for 25 min:40 s (33 min:12 s–58 min:52 s). At the beginning of the PAF (Figs. 7a–k), the activation propagated regularly on the whole atrium surface. Usually it was triggered by the foci in the left pulmonary vein (LPV) (Figs. 7 a and i) and terminated in the ARA (Figs. 7 h and k). There were conspicuous resting periods among activations, e.g. 89 ms between two successive activation in Fig. 7. On the contrast, the activation propagation seemed to be much more random during the middle of the PAF (Figs. 8a–q). Some anatomical regions activated simultaneously, e.g. the PRA and ARA in 51 min:12 s:82.5 ms and 51 min:12 s:83 ms (Figs. 8 d–g), and the LIPV and ARA in 51 min:12 s:95.5 ms (Figs. 8 m and n). In this stage, the ARA was activated individually and continuously (Figs. 8 g–k and Figs. 8 n–q). It indicated the existence of a macro-re-entry. In the end of the PAF, the reentry circuit returned to the foci triggering (not shown here).

This experiment (1) proved the conclusion of Scherlag's study [18]: the effects of autonomic ganglia stimulation at the base of RSPV can provide a substrate for the AF. (2) Indicated that the electrophysiological characteristics of myocardium might have been changed during the sustaining of PAF (remodeling), because the macro-re-entry directly relates to the repolarization gradients, i.e. dispersion of refractoriness and does not demonstrate the focal patterns at the initiation of AF. While in Scherlag's study, such remodeling was not reported [18].

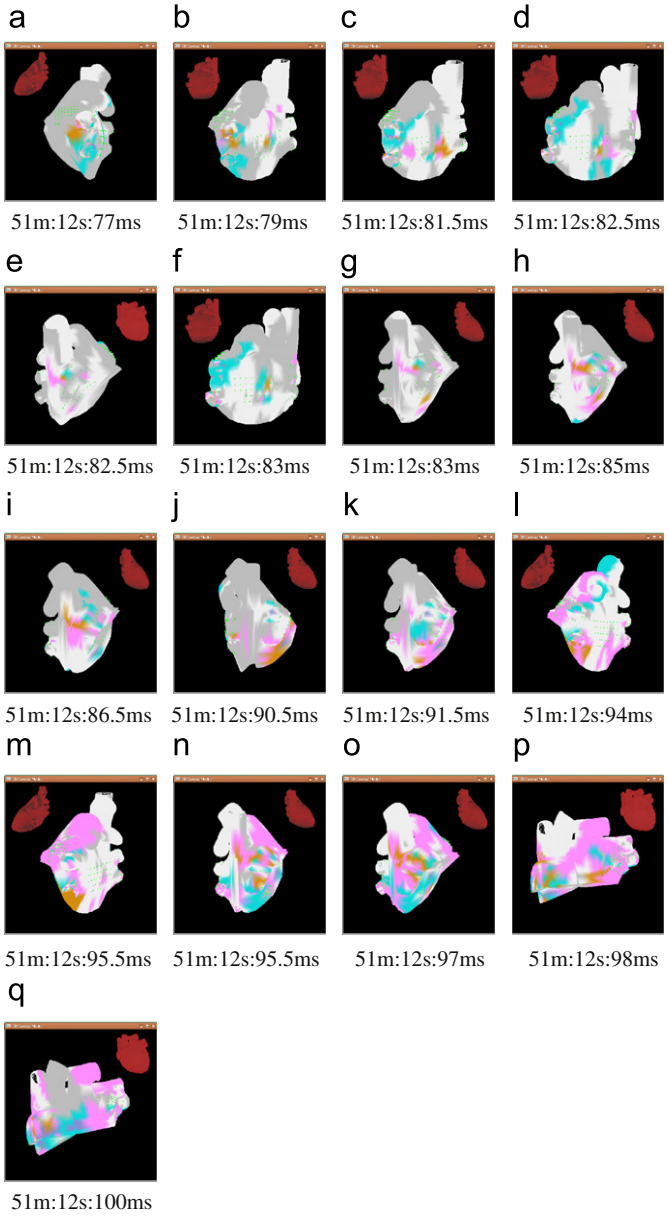

Fig. 8. Potential distribution at the middle of PAF induced by vagal simulation. Yellow region indicates the location of the activation wave front: (a) 51 min:12 s:77 ms, (b) 51 min:12 s:79 ms, (c) 51 min:12 s:81.5 ms, (d) 51 min:12 s:82.5 ms, (e) 51 min:12 s:82.5 ms, (f) 51 min:12 s:83 ms, (g) 51 min:12 s:83 ms, (h) 51 min:12 s:85 ms, (i) 51 min:12 s:86.5 ms, (j) 51 min:12 s:90.5 ms, (k) 51 min:12 s:91.5 ms, (l) 51 min:12 s:94 ms, (m) 51 min:12 s:95.5 ms, (n) 51 min:12 s:95.5 ms, (o) 51 min:12 s:97 ms, (p) 51 min:12 s:98 ms and (q) 51 min:12 s:100 ms. (For interpretation of the references to colour in this figure legend, the reader is referred to the web version of this article.)

7. Conclusion

The epicardial potential mapping gives a vivid visualization of the sequence of potential distributions on the epicardial surface, and therefore clarifies the analysis of the complex multi-channel ECG data. Cardiac experts can interpret these maps and extract a great deal of useful information for diagnosing cardiac diseases [1]. To minimize the computational complexity, the linear spatial interpolation is usually used to estimate the potential distribution on the epicardial surface from the potential measured by limited number of electrodes. However, the linear interpolating method might cause distortions, especially in the region where activation wavefront passes through [1,6]. An interpolation method based on the alignment of waveform to the local activation times [6] has been proposed to replace the former linear interpolation we used in the epicardial mapping system [4]. The source code of the implementation to this algorithm is constructed, available at http://cardiacmap.sourceforge.net/. Finally, we use this algorithm to study the mechanism of vagal AF by the same methodology of Scherlag's study, and find the macro-re-entry in the sustaining of vagal AF, which was not reported in Scherlag's study and indicates the probability of remodeling of myocardium electrophysiological characteristics.

Conflict of interest statement

None declared.

Acknowledgments

This research was supported by NSFC (National Natural Science Foundation of China, No. 30400102) and Shanghai Leading Academic Discipline Project (No. B112).

References

[1] D.H. Brooks, R.S. Macleod, Electrical imaging of the heart: electrophysiological underpinnings and signal processing opportunities, IEEE Signal Process. Mag. 14 (1997) 24–42.
[2] C. Yang, W. Lu, X. Wu, Z. Fang, Design and implementation of a new system for whole-atrial epicardial mapping, Int. J. Bioelectromagn. 9 (1) (2007) 22–23.
[3] C. Yang, W. Lu, T. Zhou, X. Wu, Z. Fang, Development of epicardial mapping system for study atrial fibrillation, in: 2008 International Conference on BioMedical Engineering and Informatics, BMEI, 2008, pp. 606–609.
[4] W. Lu, Z. Fang, A new scheme for observation and interpretation atrial fibrillation, Ann. Biomed. Eng. 26 (2008) 597–607.
[5] W. Lu, T. Zhou, C. Yang, Z. Fang, Dynamic epicardial mapping using 3D emulation, in: 2008 International Conference on BioMedical Engineering and Informatics, BMEI, 2008, pp. 420–424.
[6] N. Quan, R.S. Macleod, R.L. Lux, B. Taccardi, A novel interpolation method for electric potential fields in the heart during excitation, Ann. Biomed. Eng. 26 (1998) 597–607.
[7] D.L. Donoho, I.M. Johnstone, G. Kerkyacharian, D. Picard, Wavelet shrinkage: asymptopia? J. Roy. Stat. Soc. Ser. B. Methodological 57 (2) (1995) 301–369.
[8] M.J. Shensa, The discrete wavelet transform: wedding the "a trous" and Mallat algorithms, IEEE Trans. Signal Process. 40 (10) (1992) 2464–2482.
[9] S.G. Mallat, A theory for multiresolution signal decomposition: the wavelet representation, IEEE Trans. Pattern Anal. Mach. Intell. 11 (7) (1989) 674–693.
[10] D. Wei, Whole-heart modeling: progress, principles and applications, Prog. Biophys. Mol. Biol. 67 (1) (1997) 17–66.
[11] B.P. Bonnie, Determining the local time of activation from the unipolar electrogram: new methods, new challenges, J. Cardiovasc. Electrophysiol. 11 (10) (2000) 1129–1131.
[12] R.E. Ideker, W.M. Smith, S.M. Blanchard, et al., The assumptions of isochronal cardiac mapping, Pacing Clin. Electrophysiol. 12 (3) (1989) 456–478.
[13] B.M. Steinhaus, Estimating cardiac transmembrane activation and recovery times from unipolar and bipolar extracellular electrogram: a simulation study, Circ. Res. 64 (3) (1989) 449–462.
[14] A. Lou, C. Yang, Z. Fang, The application of multilevel B-splines in 3D emulation of dynamic epicardium, Chin. J. Med. Instrum. 29 (6) (2005) 386–398.
[15] Y.J. Chen, S.A. Chen, C.T. Tai, et al., Role of atrial electrophysiology and autonomic nervous system in patients with supraventricular tachycardia and paroxysmal atrial fibrillation, J. Am. Coll. Cardiol. 32 (1998) 732–738.
[16] F. Lombardi, D. Tarricone, F. Tundo, et al., Autonomic nervous system and paroxysmal atrial fibrillation: a study based on the analysis of RR interval changes before, during and after paroxysmal atrial fibrillation, Eur. Heart J. 25 (2004) 1242–1248.
[17] C. Chiou, J.N. Eble, D.P. Zipes, Efferent vagal innervation of the canine atria and sinus and atrioventricular nodes: the third fat pad, Circulation 95 (1997) 2573–2584.
[18] B.J. Scherlag, W.S. Yamanashi, U. Patel, et al., Autonomically induced conversion of pulmonary vein focal firing into atrial fibrillation, J. Am. Coll. Cardiol. 45 (11) (2005) 1878–1886.